

Thin films of a three-dimensional topological insulator in a strong magnetic field: a microscopic study

A. Pertsova¹, C. M. Canali¹ and A. H. MacDonald²

¹*Department of Physics and Electrical Engineering, Linnæus University, 391 82 Kalmar, Sweden*

²*Department of Physics, University of Texas at Austin, TX 78712, USA*

(Dated: today)

The response of thin films of Bi_2Se_3 to a strong perpendicular magnetic field is investigated by performing magnetic bandstructure calculations for a realistic multi-band tight-binding model. Several crucial features of Landau quantization in a realistic three-dimensional topological insulator are revealed. The $n = 0$ Landau level is absent in ultra-thin films, in agreement with experiment. In films with a crossover thickness of five quintuple layers, there is a signature of the $n = 0$ level, whose overall trend as a function of magnetic field matches the established low-energy effective-model result. Importantly, we find a field-dependent splitting and a strong spin-polarization of the $n = 0$ level which can be measured experimentally at reasonable field strengths. Our calculations show mixing between the surface and bulk Landau levels which causes the character of levels to evolve with magnetic field.

PACS numbers: 73.20.r, 71.70.Di

Keywords: topological insulator thin films, Landau levels

I. INTRODUCTION

The peculiar structure of the Landau levels (LLs) present in three-dimensional (3D) topological insulators (TIs)¹⁻³ in a strong magnetic field is a characteristic signature of their Dirac surface states⁴⁻⁶. In the simplest low-energy effective models, a field-independent $n = 0$ level emerges at the surface-state band-crossing energy that is analogous to the $n = 0$ level of another Dirac material – graphene⁷, suggesting strong similarities in the magnetic-field response of these two systems. However, a number of important features have been observed recently in thin films of binary-chalcogenide 3D TIs which indicate that the conventional picture of Landau quantization may not be fully applicable to these materials. The most notable features include (i) deviations from the square-root dependence of LL energies on magnetic field and LL index which applies when linear dispersion is present over a wide energy regime⁴, (ii) asymmetry of the LL spectrum with respect to the Dirac point^{4,5}, and (iii) finite-thickness effects, in particular the predicted splitting of the $n = 0$ level due to inter-surface coupling⁸⁻¹⁰ and its absence in ultra-thin films¹¹. LL positions are readily measured in scanning probe studies and, since they depend both on the zero-field energy bands and on the momentum-dependence of zero-field wavefunctions, are they a sensitive probe of the electronic structure.

In this work we study the electronic properties of thin films of Bi_2Se_3 in the presence of a strong quantizing magnetic field, using a microscopic approach which captures the complex electronic structure and the inter-surface hybridization of the realistic material. We perform magnetic bandstructure calculations¹²⁻¹⁴ using a multi-band tight-binding (TB) model for Bi_2Se_3 ^{15,16}. We consider slabs of 1 to 6 quintuple layers (QLs) in magnetic fields of the order of 10 T (for the smallest thickness) and larger. We find that the $n = 0$ LL is absent in

slabs with thicknesses below 5QLs but starts to emerge at this crossover thickness, in agreement with experiments on a similar system (Sb_2Te_3)¹¹. Importantly, the energy gap due to inter-surface coupling, which is found at the Dirac point of 3D TI thin films at zero field¹⁷, persists at finite magnetic fields.

This finding is partly consistent with recent theoretical studies, which investigated the effect of finite thickness on the LL spectrum either by introducing an *ad hoc* hybridization gap into the Dirac Hamiltonian of the surface states^{9,10} or by using a minimal TB model⁸ for a single-Dirac-cone family of 3D TIs. However, there are crucial differences between the results obtained with our microscopic approach and with effective models. The hybridization gap at finite magnetic fields emerges naturally in our electronic structure calculations for finite slabs. As a result, the degeneracy of the $n = 0$ level is lifted. For moderate field strengths, the gap increases approximately linearly with the field, with the dependence becoming weak with increasing thickness.

For 5QLs, the field-dependence of one of the two components of the $n = 0$ LL is in good agreement with the analytical expression derived by Liu *et al.*¹⁸ using a four-band effective Hamiltonian¹⁹. The other component, which is energetically closer to the valence band, deviates further from the analytical curve for increasing magnetic fields, with its wavefunction becoming progressively bulk-like. In the limit of small fields, the splitting approaches the value of the zero-field hybridization gap. The LLs of the bulk and surface states, which can not be easily disentangled experimentally, are identified based on the spatial character of their wavefunctions. The splitting of the $n = 0$ LL can be detected by scanning tunneling spectroscopy (STS) experiments and can be used as a probe of pertinent electronic structure features.

The paper is organized as follows. In Sec. II we describe the TB model and discuss the details of mag-

netic bandstructure calculations. The numerical results, namely the calculated LL spectra and the analysis of the hybridization gap in the presence of applied magnetic field for 1-6 QLs of Bi_2Se_3 , are presented in Sec. III. We also briefly outline possible implications of our findings for measurable electronic properties of 3D TI thin films in magnetic field. Finally, we draw some conclusions.

II. MODEL

The electronic structure of a Bi_2Se_3 slab is described by a sp^3 TB model with parameters obtained by fitting to DFT bandstructures^{15,16}. The applied magnetic field is introduced via the Peierls substitution^{20,21}. The Hamiltonian of the system reads

$$\hat{H}(\mathbf{k}) = \sum_{\substack{ii', \sigma \\ \alpha\alpha'}} \gamma_{ii'}^{\alpha\alpha'} e^{i\mathbf{k}\cdot\mathbf{r}_{ii'}} e^{-\frac{ie}{\hbar c} \int_i^{i'} \mathbf{A}\cdot d\mathbf{l}} \hat{c}_{i\alpha}^{\sigma\dagger} \hat{c}_{i'\alpha'}^{\sigma} \quad (1) \\ + \sum_{\substack{i, \sigma\sigma' \\ \alpha\alpha'}} \lambda_i \langle i, \alpha, \sigma | \hat{\vec{l}} \cdot \hat{\vec{s}} | i, \alpha', \sigma' \rangle \hat{c}_{i\alpha}^{\sigma\dagger} \hat{c}_{i\alpha'}^{\sigma'},$$

where \mathbf{k} is the reciprocal-lattice vector, $i(i')$ is the atomic index, $\alpha(\alpha')$ labels atomic orbitals, and $\sigma(\sigma')$ denotes the spin. Here i runs over all atoms in the magnetic unit cell (see definition below), while $i' \neq i$ runs over all neighbors of atom i , including atoms in the adjacent cells; $\mathbf{r}_{ii'}$ is the distance between atoms i and i' ($\mathbf{r}_{ii'}=0$ for $i=i'$). $\gamma_{ii'}^{\alpha\alpha'}$ are the Slater-Koster parameters and $\hat{c}_{i\alpha}^{\sigma\dagger}$ ($\hat{c}_{i\alpha}^{\sigma}$) is the creation (annihilation) operator for an electron with spin σ at the atomic orbital α of site i . We include the hopping between nearest neighbors in the x - y plane and next-nearest neighbors along the z -direction. The second term in Eq. (1) is the intra-atomic spin-orbit interaction, where $|i, \alpha, \sigma\rangle$ are spin- and orbital-resolved atomic orbitals, $\hat{\vec{l}}$ is the orbital angular momentum operator and $\hat{\vec{s}}$ is the spin operator; λ_i is the SO strength.

The factors $e^{i\theta_{ii'}}$, with $\theta_{ii'} = -\frac{e}{\hbar c} \int_i^{i'} \mathbf{A} \cdot d\mathbf{l}$ ($\theta_{ii}=0$), which multiply the hopping matrix elements in Eq. (1), are the Peierls phase factors. \mathbf{A} is the magnetic vector potential and \mathbf{l} is a straight path connecting the lattice sites i and i' . A uniform magnetic field is applied perpendicular to the surface of the slab, $\mathbf{B} = B\hat{z}$, and we use the Landau gauge, $\mathbf{A} = (0, B\hat{x}, 0)$. We focus on the orbital contribution of the magnetic field, which is expected to be the most crucial one for Landau quantization, at least for magnetic fields in the experimental range. Therefore we do not consider the Zeeman term. We are concerned with the effect of the hybridization between the opposite surfaces, and between the surfaces and the valence band bulk, on the LL spectrum of Bi_2Se_3 thin films.

It is known that for electrons, subject to both magnetic field and a periodic potential, the electron wavefunction can not satisfy the periodic boundary conditions (the

Hamiltonian in Eq. (1) does not commute with the operator of translations). However, one can introduce the new primitive translation vectors, which define the *magnetic unit cell*, provided that the magnetic flux ϕ threading a crystal unit cell is a rational multiple of the magnetic flux quantum $\phi_0 = hc/e$, i.e. $\phi = p\phi_0/q$, where p and q are mutually prime integers¹². The magnetic unit cell, carrying a magnetic flux $p\phi_0$, is q times larger than the crystal unit cell (see Fig. 1). The corresponding magnetic Brillouin zone is q times smaller than the original one. This *magnetic periodic boundary condition* (MPBC) requirement guarantees that the electron wavefunction only accumulates a phase $2\pi p$ when one moves along the edges of the magnetic unit cell. It follows from the MPBC that the value of the magnetic field is determined by the size of the magnetic unit cell, i.e. $B = p\phi_0/S_m = p\phi_0/qS_0$, where S_m (S_0) is the area of the magnetic (crystal) unit cell in the plane perpendicular to the field. This is a notorious numerical limitation of magnetic bandstructure calculations.

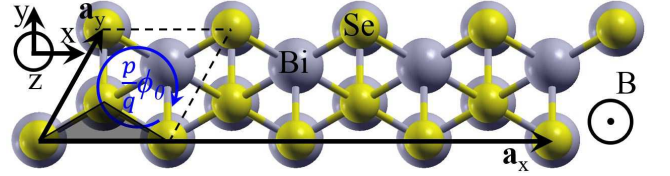


FIG. 1. Top view (x - y plane) of the magnetic unit cell ($q = 4$) of 5QLs of Bi_2Se_3 . $\mathbf{a}_{x(y)}$ are the 2D lattice vectors. Magnetic field is along the z -axis. Dashed lines show the crystal unit cell. Shaded triangle marks the elementary 2D packet.

The magnetic unit cell of a Bi_2Se_3 slab is built by replicating the slab unit cell q times along the x -axis (Fig. 1). Its size grows as $q \times (5N_{\text{QL}})$, where N_{QL} is the number of QLs. With this constraint, we were able to reach minimum field strengths of ~ 8 Tesla for 1QL and ~ 45 Tesla for 5QLs. In order to predict the behavior at smaller fields, we either use numerical fitting or, when it is appropriate, interpolate the results of our calculations between $B = 0$ and the smallest field accessible for a given thickness. We employ the Lanczos method of diagonalization at each k -point in the magnetic Brillouin zone, and focus on a small energy window around the Dirac point to reduce the computational load.

As one varies the parameter p/q , a non-trivial fractal pattern in the electronic spectrum, known as the Hofstadter butterfly²¹, emerges. First predicted for electrons on a square two-dimensional (2D) lattice, the pattern has been obtained for other 2D lattices (honeycomb²², triangular²³) and a generalization to the 3D case has been demonstrated²⁴. In this work we calculate the Hofstadter butterfly for a slab of Bi_2Se_3 with varying thickness. By focusing on the low-field (low-flux) region of the Hofstadter spectrum, which is typically the region probed in experiment, we will show the emergence of well-resolved LLs.

III. NUMERICAL RESULTS

We start with the calculation of LLs in ultra-thin films of Bi_2Se_3 . Figure 2(a) shows the Hofstadter spectrum of a 1QL-thick slab. Only the results for $\phi/\phi_0 \in [0, 1]$ are shown for better visibility. As in the case of a one-band triangular lattice model²³, the spectrum is not symmetric with respect to $\phi/\phi_0 = 1/2$ since the elementary placket, i.e. the smallest loop in the x - y plane pierced by magnetic flux, is a fraction of the unit cell (Fig. 1). At $B = 0$ there is a large energy gap, $\Delta_{B=0} = 0.84$ eV, due to inter-surface hybridization. This gap persists at finite magnetic fields. The field-dependence of the gap is quite complex, especially for large values of ϕ/ϕ_0 , where the interplay between the periodic lattice potential and the quantizing magnetic field is strong. However, in the regime where the broadening of the LLs is sufficiently weak so that few lowest levels can be resolved ($\phi/\phi_0 \lesssim 0.1$), the gap increases with magnetic field.

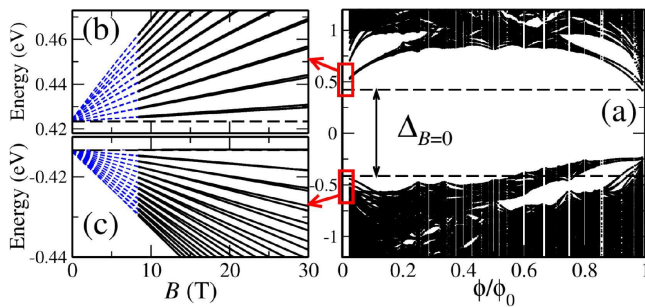


FIG. 2. (a) Hofstadter spectrum of 1QL of Bi_2Se_3 . Positive (b) and negative (c) branches of the LL spectrum (the lowest 24 levels are shown for each branch). Thin dashed lines show the results of numerical fitting for $B < 8.3$ T. Horizontal lines mark the zero-field energy gap.

We now focus on two regions of the spectrum, marked by red boxes in Fig. 2(a), corresponding to small fields ($B \leq 30$ T) and energies around the zero-field gap. There are two distinct branches of the LL spectrum, positive and negative [Fig. 2(b) and (c), respectively], with well-resolved levels. For the positive branch, the LLs come in pairs, originating from doubly degenerate states at $B = 0$. The levels disperse almost linearly with magnetic field, in striking similarity with an ordinary 2D electron gas. A similar pattern is found for the negative branch, with the exception of the top LL, which depends weakly on B in this range but starts to deflect downwards for $B > 40$ T.

In the same way, we calculate the Hofstadter spectra and the LLs for 2-6 QLs. The results are summarized in Fig. 3, where we analyze the hybridization gap as a function of magnetic field and slab thickness. Note that for $B = 10$ T we perform numerical interpolations for all thicknesses except 1QL. For $B = 45$ T an interpolation is only required for the largest thickness of 6QLs. Figure 3(a) shows that the gap increases with magnetic field for all slabs considered. The dependence is pre-

dominantly linear. By using numerical fitting, we determine numerically the linear (dominant) coefficient a_1 in the field-dependence and plot it versus the thickness in Fig. 3(b). As one can see, the field-dependence becomes weaker for thicker slabs. At the same time, the gap decreases exponentially with the thickness, as shown in Fig. 3(c). At $B = 0$ this result is well-established. However, here we explicitly demonstrate the exponential decay at finite fields. As the thickness increases beyond 5QLs, the gap becomes exponentially small and field-independent. Hence, in the limit of an infinitely-thick slab the expected LL structure, with a doubly-degenerate field-independent $n = 0$ level, is recovered.

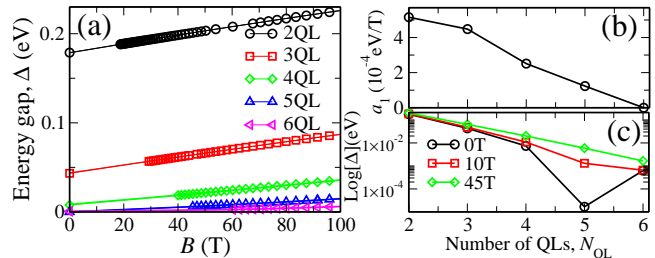


FIG. 3. (a) Hybridization gap as a function of magnetic field (including $B = 0$) for 2-6 QLs of Bi_2Se_3 . Symbols show the data points. Solid lines are numerical interpolations in the low-field region. Coefficient of the linear term in the field-dependence of the gap (b) and the logarithm of the gap (c) versus thickness for $B = 0$, 10 and 45 T.

The existence of the hybridization gap at finite magnetic fields was investigated in Ref. 8 using the low-energy model of Refs. 17 and 18. Within this approach the particle-hole symmetry is imposed from start, and therefore the model is unable to capture the asymmetry of the LL spectrum and the strong hybridization with the valence band, which is significant in Bi_2Se_3 . Our approach is free from these limitations and provides qualitatively and quantitatively accurate description of these features that are crucial in thin films.

In Ref. 8 the gap was found to depend weakly on magnetic field, oscillating as a function of the thickness, in analogy with the zero-field gap found in other continuum models^{18,25,26}. We find that at $B = 0$ the gap exhibits non-monotonic behavior at certain thicknesses, which resembles the oscillations in these continuum models. The non-monotonicity is also present at $B \neq 0$, but is smoothed out at large fields [Fig. 3(c)]. The analytical expression for the gap in Ref. 8 contains a term linear in B (multiplied by an oscillatory and exponentially decaying function of thickness). This is consistent with our calculations but only for moderate field strengths: at large fields the field-dependence in our model is highly nonlinear [Fig. 2(a)], in contrast to the result of the continuum model.

The field-dependence of LLs that we find in ultra-thin films at low magnetic fields (Fig. 2) is clearly distinct

from the square-root behavior, expected from the Dirac-Hamiltonian description of the surface states. Together with the absence of the $n = 0$ level and a sizable hybridization gap below 5QLs (Fig. 3), these results demonstrate that the Dirac fermion picture does not capture the magnetic field response of 3D TI thin films at moderate magnetic field strengths.

For typical magnetic field strengths and disorder strength, the 5QL thickness marks a crossover to the range beyond which the topologically protected bulk TI surface state is robustly manifested¹⁷. This suggests that a nearly degenerate $n = 0$ LL is expected to appear at this thickness at finite magnetic fields. The calculated LL spectrum for 5QLs is shown in Fig. 4(a). We compare our results with the analytical expression for the LLs of the surface states, obtained in Ref. 18, using a low-energy effective Hamiltonian under the assumption of decoupled bulk and surface states.

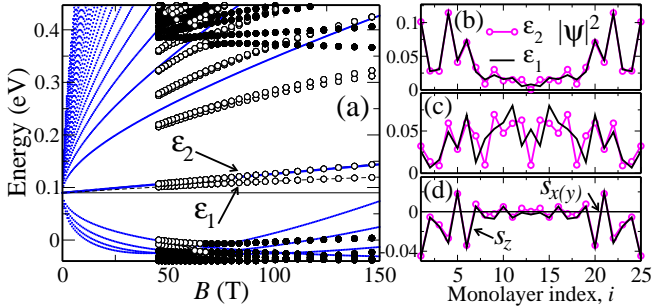


FIG. 4. (a) LL spectrum of 5QLs of Bi_2Se_3 . Open (filled) symbols are for surface (bulk) states. Dashed lines are numerical interpolations for the $n = 0$ level. Solid lines are the analytical surface LLs from Ref. 18. Horizontal line in (a) marks the position of the Dirac point at $B = 0$. Wavefunctions $|\psi|^2$ (b,c) and expectation values of the spins $s_{x(y,z)}$ (d) of the two components of the $n = 0$ LL, marked as ε_1 and ε_2 in (a), plotted versus distance along the width of the slab. In (b) and (d) $B = 45$ T, in (c) B is ten times larger.

By setting the Zeeman term to zero in the analytical formula of Liu *et al.*¹⁸, we find that the energy of the $n = 0$ level is given by $E_0 = \tilde{C}_0 + e\tilde{C}_2 B/\hbar$, where $\tilde{C}_{0(1)}$ are the parameters of the model. The term $\propto \tilde{C}_2 B$ can be traced back to the non-linear (quadratic) term $\tilde{C}_2 k^2$ in the Hamiltonian of the surface states as a function of momentum k , characteristic of the complex electronic structure of the material. Although at low fields the $n = 0$ level is nearly constant, the field-dependence becomes significant already at $B \sim 20$ T.

In our calculations at finite fields, two distinct levels with a quasi-linear dispersion emerge close to the original Dirac point. We interpret this pair of levels as the two components of $n = 0$ LL, split by inter-surface coupling. This splitting is not captured by the effective model of Ref. 18 for the surface states of a semi-infinite system. However, the field-dependence of the highest of these two levels matches remarkably well the analytical curve

(the position of the Dirac point in the analytical expression has been adjusted to that found in our calculations, i.e. ~ 0.09 eV). In the limit $B \rightarrow 0$, we expect the numerical and analytical results to converge, as confirmed by numerical interpolation (apart from a small but non-negligible gap at zero field). For the higher-index LLs, we find significant deviations from the analytical results. These features are due to the finite thickness of the sample and to higher-order non-linearities in the electronic structure that are captured by our model.

The two components of the $n = 0$ level are the true surface states, as one can see from the real-space distribution of their wavefunctions along the slab [Fig. 4(b)]. In fact, their wavefunctions are almost indistinguishable from the ones calculated at zero field. The surface-character is preserved in fields as large as 100 T. The levels have the same spin polarization and are nearly fully spin-polarized in the direction opposite to magnetic field [Fig. 4(d)]. This finding is consistent with the analytical prediction of Ref. 8. The splitting between the two $n = 0$ levels increases with magnetic field. For 5QLs, we find a splitting of 6 meV at 45 T and we estimate the splitting to be 3 meV at 20 T.

Our calculations capture the strong asymmetry of the LL spectrum with respect to the Dirac point observed in experiments^{4,5} and the mixing between bulk and surface states. The asymmetry is mainly due to the fact that the Dirac point is close to the valence band. As a result, the negative branch has only few well-resolved LLs, which merge with the bulk states with increasing magnetic field. On the contrary, the positive branch contains many levels which preserve their surface character at large fields. Based on the real-space analysis of wavefunctions, the states roughly in the energy window $[-0.02; 0.4]$ eV are surface states, while the ones outside this window are bulk states. Importantly, the character of the states does not remain constant, and some of the states evolve from surface- to bulk-like as the field increases [see Fig. 4(a)].

This behavior is due to proximity of the bulk and can be understood using the following semi-classical argument. With increasing magnetic field, the radius of the n -th Landau orbit in momentum space, expressed as $k_n = \sqrt{2|n|}/l_B$ with $l_B = \sqrt{\hbar/e|B|}$ being the magnetic length⁵, increases. Therefore, the LLs start to involve states at k -points further away from Γ . In the band-structure of a Bi_2Se_3 thin film, at $k \sim k_n$ the energy bands can be quite different from the linearly dispersed Dirac states, especially below the Dirac point, i.e. close to the valence band. Indeed, for 5QLs at $k \approx k_n$, with $k_n \approx 0.3 \text{ \AA}^{-1}$ for $B \approx 50$ T and $|n| = 1$, the bulk contribution to the energy bands just below the Dirac point becomes dominant¹⁶. This also explains why at large fields the lower component of the $n = 0$ LL deflects towards the valence band, while the upper one still follows the analytical curve. Since the lower component is energetically closer to the valence band, it is more affected by the valence-band states and at very large fields its wavefunction becomes more bulk-like [see Fig. 4(c)].

LLs manifest as peaks in the electronic density of states that can be detected in tunneling spectra measured by scanning tunneling spectroscopy (STS)^{4,5}. The energy of the $n = 0$ LL indicates the position of the Dirac point within the energy bands. A scaling analysis of LLs can be used to accurately determine the energy dispersion in 3D TIs⁵. The splitting of the $n = 0$ LL studied in this work is detectable by STS at moderate magnetic fields. Hence, it can be used as an alternative sensitive probe of the inter-surface hybridization, and in particular of the hybridization gap.

LLs are typically associated with the physics of the quantum Hall effect (QHE). The structure of LLs is embodied in the optical conductivity tensor calculated in the presence of a magnetic field, in the framework of linear response theory. This yields an estimate of the Hall conductivity in the QHE regime and allows, in general, the calculation of magneto-optical effects²⁷. We expect the features of the LLs in 3D TI thin films predicted in the present work to affect the structure and position of the Hall plateaus as function of the chemical potential^{9,10}.

IV. CONCLUSIONS

In conclusion, we presented a microscopic study of Landau quantization in thin films of Bi₂Se₃. We find that

the $n = 0$ level is absent in ultra-thin films. For a thin film containing 5QLs, the degeneracy of the $n = 0$ level is lifted due to hybridization between top and bottom surface states, with the two components being strongly spin-polarized. Since it is now possible to probe the properties of 3D TIs in strong magnetic fields ($\gtrsim 20$ T)²⁸ and to measure sub-meV gaps in thin films of 3D TIs²⁹, these spin-polarized states with a splitting of few meV can be measured experimentally. The non-trivial structure of Landau levels, originating from the realistic bandstructure and the inter-surface coupling, will affect the properties of 3D TI thin films in magnetic field, in particular magneto-optical properties, the surface quantum Hall effect and the quantum anomalous Hall effect.

ACKNOWLEDGMENTS

This work was supported by the Faculty of Natural Sciences at Linnaeus University and by the Swedish Research Council under Grant Number: 621-2010-3761. AHM was supported by the Welch Foundation under Grant No. TBF1473 and by the DOE Division of Materials Sciences and Engineering under grant No. DE-FG03-02ER45958. Computational resources have been provided by the Lunarc center for scientific and technical computing at Lund University.

-
- ¹ M. Z. Hasan and C. L. Kane, *Rev. Mod. Phys.* **82**, 3045 (2010).
 - ² X.-L. Qi and S.-C. Zhang, *Rev. Mod. Phys.* **83**, 1057 (2011).
 - ³ D. Hsieh, Y. Xia, D. Qian, L. Wray, J. H. Dil, F. Meier, J. Osterwalder, L. Patthey, J. G. Checkelsky, N. P. Ong, A. V. Fedorov, H. Lin, A. Bansil, D. Grauer, Y. S. Hor, R. J. Cava, and M. Z. Hasan, *Nature* **460**, 1101 (2009).
 - ⁴ P. Cheng, C. Song, T. Zhang, Y. Zhang, Y. Wang, J.-F. Jia, J. Wang, Y. Wang, B.-F. Zhu, X. Chen, X. Ma, K. He, L. Wang, X. Dai, Z. Fang, X. Xie, X.-L. Qi, C.-X. Liu, S.-C. Zhang, and Q.-K. Xue, *Phys. Rev. Lett.* **105**, 076801 (2010).
 - ⁵ T. Hanaguri, K. Igarashi, M. Kawamura, H. Takagi, and T. Sasagawa, *Phys. Rev. B* **82**, 081305 (2010).
 - ⁶ Y. Okada, W. Zhou, C. Dhital, D. Walkup, Y. Ran, Z. Wang, S. D. Wilson, and V. Madhavan, *Phys. Rev. Lett.* **109**, 166407 (2012).
 - ⁷ J. Martin, N. Akerman, G. Ulbricht, T. Lohmann, K. von Klitzing, J. H. Smet, and A. Yacoby, *Nat. Phys.* **5**, 669 (2009).
 - ⁸ Z. Yang and J. H. Han, *Phys. Rev. B* **83**, 045415 (2011).
 - ⁹ A. A. Zyuzin and A. A. Burkov, *Phys. Rev. B* **83**, 195413 (2011).
 - ¹⁰ M. Tahir, K. Sabeeh, and U. Schwingenschlgl, *Journal of Applied Physics* **113**, 043720 (2013).
 - ¹¹ Y. Jiang, Y. Wang, M. Chen, Z. Li, C. Song, K. He, L. Wang, X. Chen, X. Ma, and Q.-K. Xue, *Phys. Rev. Lett.* **108**, 016401 (2012).
 - ¹² E. Brown, *Phys. Rev.* **133**, A1038 (1964).
 - ¹³ F. A. Butler and E. Brown, *Phys. Rev.* **166**, 630 (1968).
 - ¹⁴ M. Graf and P. Vogl, *Phys. Rev. B* **51**, 4940 (1995).
 - ¹⁵ K. Kobayashi, *Phys. Rev. B* **84**, 205424 (2011).
 - ¹⁶ A. Pertsova and C. M. Canali, *New Journal of Physics* **16**, 063022 (2014).
 - ¹⁷ Y. Zhang, K. He, C.-Z. Chang, C.-L. Song, L.-L. Wang, J.-F. Chen, X. amd Jia, Z. Fang, X. Dai, W.-Y. Shan, S.-Q. Shen, Q. Niu, X.-L. Qi, S.-C. Zhang, X.-C. Ma, and Q.-K. Xue, *Nat. Phys.* **6**, 584 (2010).
 - ¹⁸ C.-X. Liu, X.-L. Qi, H.-J. Zhang, X. Dai, Z. Fang, and S.-C. Zhang, *Phys. Rev. B* **82**, 045122 (2010).
 - ¹⁹ H.-J. Zhang, C.-X. Liu, X.-L. Qi, X.-Y. Deng, X. Dai, S.-C. Zhang, and Z. Fang, *Phys. Rev. B* **80**, 085307 (2009).
 - ²⁰ R. Peierls, *Z. Phys* **80**, 763 (1933).
 - ²¹ D. R. Hofstadter, *Phys. Rev. B* **14**, 2239 (1976).
 - ²² R. Ramal, *J. Physique* **46**, 1345 (1985).
 - ²³ G.-Y. Oh, *Phys. Rev. B* **63**, 087301 (2001).
 - ²⁴ M. Koshino, H. Aoki, K. Kuroki, S. Kagoshima, and T. Osada, *Phys. Rev. Lett.* **86**, 1062 (2001).
 - ²⁵ J. Linder, T. Yokoyama, and A. Sudbø, *Phys. Rev. B* **80**, 205401 (2009).
 - ²⁶ H.-Z. Lu, W.-Y. Shan, W. Yao, Q. Niu, and S.-Q. Shen, *Phys. Rev. B* **81**, 115407 (2010).
 - ²⁷ W.-K. Tse and A. H. MacDonald, *Phys. Rev. B* **84**, 205327 (2011).
 - ²⁸ J. G. Analytis, R. D. McDonald, S. C. Riggs, J. H. Chu, G. S. Boebinger, and I. R. Fisher, *Nat. Phys.* **6**, 960 (2010).
 - ²⁹ D. Kim, P. Syers, N. P. Butch, J. Paglione, and M. S. Fuhrer, *Nat. Commun.* **4**, 2040 (2013).